Applied Physics Letters

Simulations for InAlAs digital alloy avalanche photodiodes

Cite as: Appl. Phys. Lett. **115**, 171106 (2019); https://doi.org/10.1063/1.5114918
Submitted: 22 June 2019 . Accepted: 10 October 2019 . Published Online: 23 October 2019

J. Zheng, Y. Yuan, Y. Tan, Y. Peng, A. Rockwell, S. R. Bank, A. W. Ghosh, and J. C. Campbell

Applied Physics Letters ARTICLE scitation.org/journal/apl

Simulations for InAlAs digital alloy avalanche photodiodes

Cite as: Appl. Phys. Lett. **115**, 171106 (2019); doi: 10.1063/1.5114918
Submitted: 22 June 2019 · Accepted: 10 October 2019 ·
Published Online: 23 October 2019

View Online Export Citation CrossMark

J. Zheng,[1] Y. Yuan,[1] Y. Tan,[1,a)] Y. Peng,[1] A. Rockwell,[2] S. R. Bank,[2] A. W. Ghosh,[1,3] and J. C. Campbell[1,b)]

AFFILIATIONS

[1]Department of Electrical and Computer Engineering, University of Virginia, Charlottesville, Virginia 22904, USA
[2]Microelectronics Research Center, University of Texas, Austin, Texas 78758, USA
[3]Department of Physics, University of Virginia, Charlottesville, Virginia 22904, USA

[a)]Present address: Synopsys, Inc., 455 N Mary Ave, Sunnyvale, California 94085, USA.
[b)]**Author to whom correspondence should be addressed:** jcc7s@eservices.virginia.edu

ABSTRACT

3D band structure-based Monte Carlo simulations have been utilized to simulate InAlAs digital alloy avalanche photodiodes. The simulated current–voltage curve and excess noise factor fit well with experimental results. Ionization coefficients calculated by the Monte Carlo technique were incorporated into the recurrence model, which is easier to implement and requires less computation time.

Driven by the development of the internet, datacenters, and fiber optic telecommunications, avalanche photodiodes (APDs) have become key optoelectronic components owing to their high sensitivity.[1] However, the performance of APDs in the short-wavelength infrared (SWIR) still lags behind that of Si in the visible[2,3] and InAs[4,5] and HgCdTe[6,7] in the midwave infrared (MWIR). One reason for this is that the materials that, to date, have been available for SWIR APDs, such as InGaAs/InP, InGaAs/InAlAs, and Ge/Si, have not achieved the low noise of their visible and MWIR counterparts.[1] The primary noise component, the shot noise, can be expressed as $\langle i^2 \rangle = 2qIM^2F(M)\Delta f$,[8] where I is the total photocurrent and dark current, M is the average multiplication gain, and Δf is the bandwidth. The excess noise factor, $F(M)$, is a result of the random nature of impact ionization; in the local field model, when avalanche is caused by pure electron injection, it is given by $F(M) = kM + (1\text{-}k)(2\text{–}1/M)$, where k is the ratio of the hole ionization coefficient, β, to that of the electron, α.[8] If avalanche is caused by pure hole injection, the equation will have k replaced by $1/k$. While according to the excess noise factor measurement, InAs and HgCdTe exhibit $k = 0$, the k values for InP and InAlAs are ~0.45[9] and 0.2,[10] respectively, which can result in significantly higher noise. Although Si exhibits low k (~0.02), the lattice mismatch in Ge/Si APDs gives rise to high dark current, which obviates Si's low excess noise.[1] Recently, AlInAsSb digital alloy separate absorption, charge, and multiplication (SACM) APDs have achieved low excess noise ($k \sim 0.01$) in the SWIR.[11,12] The digital alloy lattice structure is considered a key aspect of this performance improvement. It has also been shown that the InAlAs digital alloy exhibits lower k compared to the InAlAs random alloy.[13–15] Recently, the band structure of 6 monolayer (ML) InAlAs digital alloy has been calculated using an empirical tight binding method.[13,15] In this paper, Monte Carlo simulation based on the calculated 3D band structure is used to study the APD characteristics. 3D meshes ($19 \times 19 \times 19$) were taken within the first Brillouin zone; 46 conduction bands and 24 valence bands were included. A detailed description of the band structure calculation is provided in Refs. 13 and 15.

The most important scattering mechanisms, deformation scattering, and impact ionization are included in the Monte Carlo simulation. It should be noted that deformation scattering includes optical and acoustic phonon inner- and inter-valley scattering. Between scattering events, carrier transport is considered to be free flight. The Fermi Golden Rule is used to calculate the deformation scattering rate $P^{def}_{\nu\nu',\eta}(\boldsymbol{k}, \Omega_{\boldsymbol{k}\pm\boldsymbol{q}})$ from a point $\boldsymbol{k}$ in band ν to a region $\Omega_{\boldsymbol{k}'}$ and in band ν' centered around $\boldsymbol{k}'$, which can be expressed as[16,17]

$$P^{def}_{\nu\nu',\eta}(\boldsymbol{k}, \Omega_{\boldsymbol{k}\pm\boldsymbol{q}}) = \frac{\pi}{\rho\omega_{\eta q}} \left|\Delta^{\eta}(\nu', \boldsymbol{k}, \boldsymbol{q}, \nu)\right|^2 \left|I(\nu, \nu'; \boldsymbol{k}, \boldsymbol{k}\pm\boldsymbol{q})\right|^2 \times D_{\nu}(E', \Omega_{\boldsymbol{k}'}) \left(N_{\eta q} + \frac{1}{2} \mp \frac{1}{2}\right), \quad (1)$$

where ρ is the lattice density, $\boldsymbol{q}$ is the phonon wave vector of mode η, and $\Delta^{\eta}(\nu', \boldsymbol{k}, \boldsymbol{q}, \nu)$ is the deformation potential, which is taken to be 0.83 eV/Å in the conduction band and 0.31 eV/Å in the valence band for this calculation.[13] $I(\nu, \nu'; \boldsymbol{k}, \boldsymbol{k} \pm \boldsymbol{q})$ is the overlap integral between

the initial and final states, and $D_{\nu'}(E', \Omega_{k'})$ is the density of states in $\Omega_{k'}$, at energy $E' = E(k) \pm \hbar\omega_{\eta q}$. The optical and acoustic phonon energies, 36.4 and 16.5 meV, respectively, are the averages of those for InAs (acoustic: 14.4 meV; optical: 28.6 meV) and AlAs (acoustic: 18.6 meV; optical: 44.2 meV).[18]

Impact ionization rates (R_{ii}) are calculated using the Keldysh model, which can be expressed as[19]

$$P_{\nu\nu'}(\boldsymbol{k}, \boldsymbol{k}') = S(E - E_{th})^{\gamma}. \tag{2}$$

The Keldysh parameters for electrons and holes are given in Table I.

The mean energies of the secondary generated carriers after impact ionization triggered by an electron with energy E_c and a hole with energy E_v are expressed as[20]

$$\langle E_c' \rangle(E_c) = mE_c + s, \tag{3}$$

$$\langle E_v' \rangle(E_v) = mE_v + s, \tag{4}$$

where $\langle E_c' \rangle$ and $\langle E_v' \rangle$ correspond to the total energy of indistinguishable secondary carriers. The parameters m and s are taken to be 0.384 and −0.518 eV in this work.[20] If the impact ionization is triggered by an electron, the energies of the three carriers (primary electron and generated electron–hole pair) after ionization are[19]

$$E_{e1}' = \langle E_c' \rangle(E_c)\varepsilon, \tag{5}$$

$$E_{e2}' = \langle E_c' \rangle(E_c)(1 - \varepsilon), \tag{6}$$

$$E_h' = E_c - \langle E_c' \rangle(E_c) - E_g, \tag{7}$$

where $0 < \varepsilon < 1$ is a random number and E_g is the bandgap of the material, which is 1.24 eV. If the impact ionization is triggered by a hole, the energies of the three carriers (primary hole and generated electron–hole pair) after ionization are[19]

$$E_{h1}' = \langle E_c' \rangle(E_c)\varepsilon, \tag{8}$$

$$E_{h2}' = \langle E_c' \rangle(E_c)(1 - \varepsilon), \tag{9}$$

$$E_e' = E_v - \langle E_v' \rangle(E_v) - E_g. \tag{10}$$

A 6 ML InAlAs digital alloy APD with a multiplication layer thickness of 600 nm was analyzed using the Monte Carlo method described above and compared with experimental results to verify the key parameters. The electric field is assumed to be uniform across the multiplication region for bias in the range of 0 to 34 V.

The Monte Carlo model was used to calculate the electron and hole ionization coefficients by following the transport of an electron and a hole for a distance of 100 μm, which is sufficient for this calculation. The electron (α) and hole (β) ionization coefficients were calculated as the inverse of the average interval between impact ionizations. The results are shown in Fig. 1.

TABLE I. Electron and hole parameters in the Keldysh model.

	S (1/s)	E_{th} (eV)	γ (arbitrary)
Electron	2×10^{17}	1.6	1
Hole	5×10^{14}	1.46	1

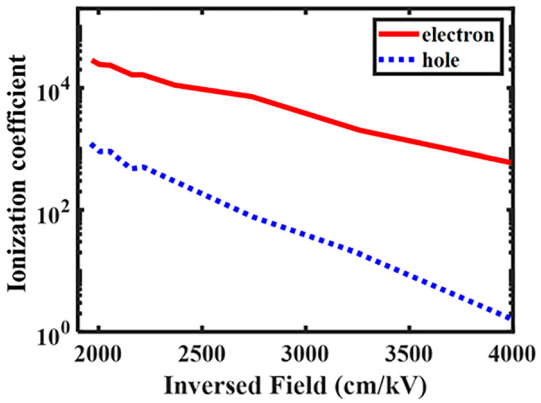

FIG. 1. Simulation of electron and hole impact ionization coefficients in 6 ML InAlAs digital alloy.

Then, the gain and excess noise are simulated and shown in Fig. 2. 1000 initial electrons were injected into the multiplication layer. The total number of ionization generated carriers, M, by each injected carrier is recorded. The gain, G, is taken to be the average value of M. The excess noise factor, F, is calculated by

$$F = \frac{\langle M^2 \rangle}{\langle M \rangle^2}. \tag{11}$$

Compared to the 3D band structure-based Monte Carlo simulation, the recurrence model provides a more time efficient way to simulate the gain and excess noise. Ionization coefficients determined by the Monte Carlo simulation can be directly incorporated into analytical approaches such as the recurrence technique. In this paper, the ionization coefficients calculated by Monte Carlo simulation are used in the analytical recurrence model [Eqs. (12)–(23)] to calculate the gain and excess noise factor and compare with experimental results and the Monte Carlo simulation. $Z(x)$ and $Y(x)$ are defined as the total secondary carriers (electrons and holes, respectively) generated by a single initial electron (hole) at the point x in the multiplication region. The parameters $z(x)$ and $y(x)$ are the statistical averages of $Z(x)$ and $Y(x)$ and can be expressed as[21]

$$z(x) = \left[1 - \int_0^{W-x} h_e(\xi)d\xi\right] + \int_x^W \left[2z(\xi) + y(\xi)\right] h_e(\xi - x)d\xi, \tag{12}$$

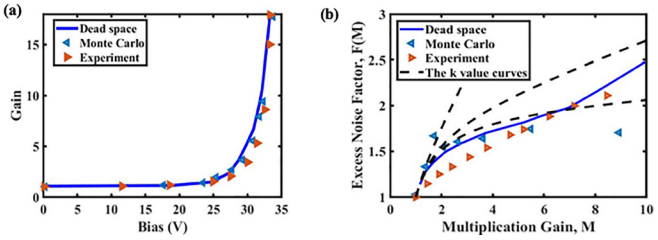

FIG. 2. Recurrence model, Monte Carlo simulations, and measurements. (a) Gain vs bias voltage and (b) excess noise factor vs gain.

$$y(x) = \left[1 - \int_0^x h_h(\xi)d\xi\right] + \int_0^x \left[2y(\xi) + z(\xi)\right]h_h(x-\xi)d\xi, \quad (13)$$

where W is the total thickness of the multiplication region and $h_e(x)$ and $h_h(x)$ are the ionization probability density functions for electrons and holes and can be expressed as[22]

$$h_e(x) = \alpha^* e^{-\alpha^*(x-d_e)}u(x-d_e), \quad (14)$$

$$h_h(x) = \beta^* e^{-\beta^*(x-d_h)}u(x-d_h), \quad (15)$$

$$\frac{1}{\alpha} = d_e + \frac{1}{\alpha^*}, \quad (16)$$

$$\frac{1}{\beta} = d_h + \frac{1}{\beta^*}, \quad (17)$$

where α and β are the ionization coefficients calculated from the Monte Carlo Method as shown in Fig. 1. α^* and β^* denote the enabled ionization coefficient. The detailed discussion on Eqs. (16) and (17) can be found in Ref. 22. $u(x)$ is the unit step function, which is equal to 1 when $x > 0$ or 0 when $x \leq 0$. d_e and d_h are the dead spaces for electrons and holes, respectively, which can be expressed as[20]

$$d_e = \frac{E_{ie}}{q\mathrm{E}}, \quad (18)$$

$$d_h = \frac{E_{ih}}{q\mathrm{E}}, \quad (19)$$

where E_{ie} and E_{ih} and are the impact ionization threshold energies, q is the electron charge, and E is the electric field strength.

The multiplication gain is obtained from the expression[21]

$$\langle G\rangle = \frac{1}{2} \times [z(0) + 1], \quad (20)$$

and the excess noise factor is given by[20]

$$F = \frac{z_2(0) + 2z(0) + 1}{[z(0) + 1]^2}, \quad (21)$$

where $z_2(x)$ and $y_2(x)$ are the statistic averages of the second moments of Z(x) and Y(x), respectively, and can be written as[21]

$$z_2(x) = \left[1 - \int_0^{W-x} h_e(\xi)d\xi\right] + \int_x^W \left[2z_2(\xi) + y_2(\xi) + 4z(\xi)y(\xi) + 2z^2(\xi)\right]h_e(\xi - x)d\xi, \quad (22)$$

$$y_2(x) = \left[1 - \int_0^x h_h(\xi)d\xi\right] + \int_0^x \left[2y_2(\xi) + z_2(\xi) + 4z(\xi)y(\xi) + 2y^2(\xi)\right]h_h(x-\xi)d\xi. \quad (23)$$

Iterative numerical methods are used to solve Eqs. (12), (13), (20) and (21) to obtain the gain and excess noise factors.

The measured, Monte Carlo simulated, and recurrence model calculated gain vs bias voltage results are plotted in Fig. 2(a) as dotted, dashed, and solid curves, respectively; good agreement is observed. Figure 2(b) shows the experimental (▶), Monte Carlo (◀), and recurrence model (solid line) excess noise factor vs gain. The McIntyre model[8] expressed as $F(M) = kM + (1-k)(1-1/M)$ provides reference curves for different k values. It can be seen that the calculation results indicate a low k value at the same level with the experimental results ($k \approx 0.02$), which were reported in Ref. 13. From Fig.1, we can see that the ionization coefficient of electrons is much larger than that of holes, and so the k value is approaching 0. However, a deviation of excess noise between simulation results and experimental results still exists. We believe that this is due to the simplification in Monte Carlo simulation, which are (a) we only considered the deformation scattering and impact ionization, (b) the deformation potential is constant in the valence band, and (c) an empirical Keldysh model is used in calculating the impact ionization rate.

In this paper, we provide a primary calculation of the ionization coefficient and compared it with only one structure. A further verification with more samples is necessary. Moreover, 3D band structure-based Monte Carlo simulations were used to characterize the gain, excess noise, and gain-bandwidth product of a 6 ML InAlAs digital alloy APD. The simulations agree well with experimental results. Ionization coefficients were also calculated using Monte Carlo simulation and were used in a recurrence model to calculate gain and excess noise, which agreed with the experimental measurements, providing a more time efficient way to simulate the 6 ML InAlAs digital alloy-based APD.

This work was supported by the Army Research Office (No. W911NF-17-1-0065) and DARPA (No. GG11972.153060).

REFERENCES

[1]J. C. Campbell, J. Lightwave Technol. **34**, 278 (2016).
[2]M. Huang, S. Li, P. Cai, G. Hou, T. Su, W. Chen, C. Hong, and D. Pan, IEEE J. Sel. Top. Quantum. Electron. **24**, 11 (2018).
[3]W. N. Grant, Solid-State Electron. **16**, 1189 (1973).
[4]A. R. J. Marshall, C. Tan, M. J. Steer, and J. P. R. David, Appl. Phys. Lett. **93**, 111107 (2008).
[5]A. R. J. Marshall, P. J. Ker, A. Krysa, J. P. R. David, and C. Tan, Opt. Express **19**, 23341 (2011).
[6]J. D. Beck, C. Wan, M. A. Kinch, and J. E. Robinson, Proc. SPIE **4455**, 188 (2001).
[7]J. Beck, C. Wan, M. Kinch, J. Robinson, P. Mitra, R. Scritchfield, F. Ma, and J. Campbell, J. Electron. Mater. **35**, 1166 (2006).
[8]R. J. McIntyre, IEEE Trans. Electron Devices **ED13**, 164 (1966).
[9]C. A. Armiento and S. H. Groves, Appl. Phys. Lett. **43**, 198 (1983).
[10]N. Li, R. Sidhu, X. W. Li, F. Ma, X. G. Zheng, S. L. Wang, G. Karve, S. Demiguel, A. L. Holmes, and J. C. Campbell, Appl. Phys. Lett. **82**, 2175 (2003).
[11]M. Ren, S. J. Maddox, M. E. Woodson, Y. J. Chen, S. R. Bank, and J. C. Campbell, Appl. Phys. Lett. **108**, 191108 (2016).
[12]M. E. Woodson, M. Ren, S. J. Maddox, Y. Chen, S. R. Bank, and J. C. Campbell, Appl. Phys. Lett. **108**, 081102 (2016).
[13]J. Zheng, Y. Yuan, Y. Tan, Y. Peng, A. K. Rockwell, S. R. Bank, A. W. Ghosh, and J. C. Campbell, J. Lightwave Technol. **36**, 3580 (2018).
[14]Y. Yuan, J. Zheng, Y. Tan, Y. Peng, A. K. Rockwell, S. R. Bank, A. W. Ghosh, and J. C. Campbell, Photonics Res. **6**, 794 (2018).
[15]J. Zheng, Y. Tan, Y. Yuan, A. W. Ghosh, and J. C. Campbell, J. Appl. Phys. **125**, 082514 (2019).
[16]J. Zheng, L. Wang, X. Wu, Z. Hao, C. Sun, B. Xiong, Y. Luo, Y. Han, J. Wang, H. Li, J. Brault, S. Matta, M. Al Khalfioui, J. Yan, T. Wei, Y. Zhang, and J. Wang, Appl. Phys. Lett. **109**, 241105 (2016).

[17]J. Y. Zheng, L. Wang, X. Z. Wu, Z. B. Hao, C. Z. Sun, B. Xiong, Y. Luo, Y. J. Han, J. Wang, H. T. Li, M. Li, J. B. Kang, and Q. Li, Appl. Phys. Express **10**, 071002 (2017).
[18]L. Lindsay, D. A. Broido, and T. L. Reinecke, Phys. Rev. B **87**, 165201 (2013).
[19]F. Osaka and T. Mikawa, IEEE J. Quantum Electron. **22**, 471 (1986).
[20]D. Dolgos, A. Schenk, and B. Witzigmann, J. Appl. Phys. **111**, 073714 (2012).
[21]M. A. Saleh, M. M. Hayat, B. E. A. Saleh, and M. C. Teich, IEEE Trans. Electron Devices **47**, 625 (2000).
[22]J. S. Cheong, M. M. Hayat, X. X. Zhou, and J. P. R. David, IEEE Trans. Electron Devices **62**, 1949 (2015).